Matrix isolation ESR and theoretical studies of metal phosphides

Rebecca O. Fuller,[a] Graham S. Chandler, Jeffrey R. Davis, and Allan J. McKinley
Chemistry M313, School of Biomedical, Biomolecular and Chemical Sciences, University of Western Australia, 35 Stirling Highway, Crawley, Western Australia 6009, Australia

(Received 9 July 2010; accepted 30 August 2010; published online 26 October 2010)

The ZnP, ^{67}ZnP, CdP, ^{111}CdP, and ^{113}CdP radicals have been formed by laser ablation of the metal with GaP pressed into the metal surface, isolated in an inert neon matrix at 4.3 K and their electronic structure was established using electron spin resonance spectroscopy. The following magnetic parameters were determined experimentally for ZnP/^{67}ZnP, $g_{\perp}=1.9982(2)$, $A_{\perp}(P)=111(6)$ MHz, $A_{\perp}(^{67}Zn)=160(2)$ MHz, and $D=-29\,988(3)$ MHz and estimates were made for the following ZnP/^{67}ZnP magnetic parameters: $g_{\parallel}=1.9941(2)$, $A_{\parallel}(P)=-5(6)$ MHz, and $A_{\parallel}(^{67}Zn)=180(50)$ MHz. The following magnetic parameters for CdP/^{111}CdP/^{113}CdP were determined experimentally: $g_{\perp}=1.9963(2)$, $A_{\perp}(P)=97(3)$ MHz, $A_{\perp}(^{111}Cd)=862(3)$ MHz, and $A_{\perp}(^{113}Cd)=902(3)$ MHz. Evidence for the formation of the MgP radical was also obtained and an approximate hyperfine coupling constant of $A_{\perp}(P)=157(6)$ MHz was determined. The low-lying electronic states of ZnP and MgP were also investigated using the multiconfigurational self-consistent field technique. Potential energy surfaces, binding energies, optimized bond lengths, energy separations, and dissociation energies have been determined. Both radicals are found to have $^4\Sigma^-$ ground states with a leading configuration at r_e of $10\sigma^2 11\sigma^2 5\pi^1 5\pi^1 12\sigma^1$ for ZnP and $7\sigma^2 8\sigma^2 3\pi^1 3\pi^1 9\sigma^1$ for MgP. Significant mixing to this state is calculated for MgP. © *2010 American Institute of Physics*. [doi:10.1063/1.3491501]

I. INTRODUCTION

Considerable interest has been shown in the production and spectroscopy of Groups III–V semiconductors.[1–4] Theoretical and experimental investigations[5–11] of such species can provide insight into their properties. Furthermore, an understanding of the formation processes and the fundamentals of bonding for these types of molecules will help improve the quality and performance of devices grown. The conduction and carrier type in semiconductors are greatly affected by the addition of impurities or dopants at the interstitial sites or as complexes. Groups III–V semiconductors like InP and GaAs can be doped with both electron accepting and donating species depending on which lattice site the impurity occupies.[12] Group II elements like Mg, Zn, and Cd tend to act as acceptors by occupying the cation site of the group III atom. There is a good understanding about the conditions affecting the incorporation of the impurities and the resultant physical and chemical properties of the doped material.[12] However, very little spectroscopic information for the interaction between the metal dopant and the phosphorus atom exists in the literature, prompting this work.

In this study the radicals of ZnP, MgP, and CdP have been investigated in a similar manner to the monomethyl metal radicals published earlier.[13–16] ZnP and CdP have been isolated in a neon matrix and studied by electron spin resonance (ESR) spectroscopy. For ZnP/^{67}ZnP the values for $g_{\perp}$, $A_{\perp}(P)$, $A_{\perp}(^{67}Zn)$, and D have been determined and values derived for $g_{\parallel}$, $A_{\parallel}$, and $A_{\parallel}(^{67}Zn)$. For CdP/^{111}CdP/^{113}CdP, $g_{\perp}$, $A_{\perp}(P)$, $A_{\perp}(^{111}Cd)$, and $A_{\perp}(^{113}Cd)$ were determined experimentally. In addition, evidence for the formation of the MgP radical was also obtained by this aforementioned method and an approximate hyperfine coupling constant of $A_{\perp}(P)$ was obtained. The inability to form this species in high yields prompted us to conduct a theoretical investigation of the electronic structure of the radical. Boldyrev and Simons,[17,18] undertook *ab initio* calculations on the ZnP and MgP radicals. They predicted that the electronic ground state of these molecules has three unpaired electrons, that is a $^4\Sigma^-$ state.

Unlike closed shell molecules, radicals are often not well described by simple single determinant wavefunctions.[19] Constructing a wavefunction involving several electronic states is more appropriate.[19] A number of research groups have carried out systematic theoretical studies using multiconfigurational techniques, multiconfigurational self-consistent field (MCSCF)/multireference singles and double configuration interaction (MRSDCI) on a number of groups III–V radicals. Balasubramanian and co-workers investigated Ga_xAs_y,[20] Ga_xP_y,[21,22] In_xP_y,[23,24] Al_xP_y,[25] Ga_xN_y,[26] and In_xN_y.[11,27] Das and co-workers studied GaAs,[28] GaP,[29] InSb,[30] GaSb,[31] InP,[32] InAs,[33] GaBi,[34] InBi,[35] AlSb,[36] TlAs,[37] TlSb,[37] and TlBi.[37] These studies have demonstrated that the ground and low-lying electronic states of these species have significant electron correlation and are multireference in nature. Single configuration techniques like Møller-Pesser perturbation theory (MP2) and density functional theory (DFT) are likely to be inadequate for describing the materials of this type. Despite the large amount of literature for theoretical studies into the electronic nature of groups III–V semiconductors, no such studies have been performed for the doped species. In this work, an investigation into the low-lying

[a]Electronic mail: becky@cyllene.uwa.edu.au.

electronic states of both ZnP and MgP using a multiconfigurational method is conducted. Potential energy surfaces for each radical were constructed for the seven lowest electronic states, with two pairs of degenerate states.

II. EXPERIMENTAL

The design of the main vacuum system and apparatus used for the neon matrix experiments has been published previously.[13] Only a brief description of the methodology for this experiment will be given here. The radicals were generated by laser ablation of a metal target, either zinc (Asia Pacific Specialty Chemicals, Impurities: iron 0.002%), magnesium (Aldrich 99.9+%), or cadmium (Koch-Light Laboratories, Ltd. 99.999%), which was doped by pressing (3–5 tons/load) finely crushed gallium phosphide (Aldrich 99.99%) crystals into the metal target. A frequency doubled, pulsed 532 nm Nd:YAG (yttrium aluminum garnet) laser (Surelite I) was used in all experiments. The laser has a pulse length of 8 ns and was operated at 10 Hz with an energy of 15 mJ/pulse. The beam was focused to a small spot (<0.5 mm in radius) through a 7.5 cm focal length lens. The laser was continuously moved over the metal target surface during the deposition process and vaporized the metal and gallium phosphide surface. The metal target was in a vacuum chamber along with the copper deposition target. The "plume" formed by the vaporization expanded into the vacuum and was then trapped in a neon matrix deposited onto a copper deposition target that was maintained at 4.3 K by a continuous-flow liquid-helium cryostat (Cryo Industries of America RC110). High purity neon was injected at a flow rate of about 8 SCCM (SCCM denotes standard cubic centimeter per minute at STP) into the vacuum chamber through a port directed at the deposition target. Deposition times varied from 45 to 60 min depending on the reactant metal used. Background system pressures ranged from 2.5 to 4 $\times 10^{-7}$ Torr before cooling of the cryostat. ESR spectra of the resultant matrix were then recorded on a Bruker ESP300E spectrometer with a DM4116 cavity.

Spectral analysis was performed by exact diagonalization of the spin Hamiltonian with the GEN program.[38,39] The uncertainties in the magnetic parameters were estimated by adjusting these parameters to minimize the sum of the squares of the difference between observed and calculated peak positions. These uncertainties are given in the brackets next to the calculated parameters. The uncertainty margin and the range it encompassed was taken to be sufficiently large enough so that the maximum and minimum values gave calculated peak positions that differed substantially from those observed.

Ab initio calculations were performed using GAMESS(US) (Ref. 40) to study the low-lying electronic states of MgP and ZnP. Calculations using the full valence MCSCF level of theory were performed with a correlation consistent polarized valence double zeta (cc-pVDZ)[41–45] basis set for both magnesium and phosphorus (12s 8p 1d/4s 3p 1d) in MgP. For ZnP, a triple zeta valence (TZV)[46,47] basis set with additional p, d, and f functions for both zinc (14s 12p 6d 1f/10s 9p 4d 1f) and phosphorus (12s 9p 1d 1f/4s 4p 1d 1f) was employed. We did not employ the frozen core approximation in our calculations. The active space in calculations of electrons spanning eight orbitals. In particular, the $10\sigma 11\sigma 5\pi 5\pi 12\sigma$ orbitals for ZnP and the $7\sigma 8\sigma 3\pi 3\pi 9\sigma$ orbitals for MgP were used in the calculation. This active space was chosen on energetic grounds.

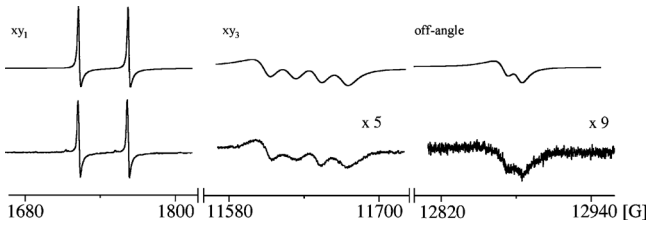

FIG. 1. The lower trace shows the ESR spectra for the ZnP radical isolated in a neon matrix at 4.3 K after annealing to 9.3 K. Spectra were recorded at a microwave power of 20 mW and at a frequency for the xy_1, xy_3, and OA of 9715.864 MHz, 9708.799 MHz, and 9715.701 MHz, respectively. The upper trace gives the simulated ESR spectrum for the ZnP radical obtained using the magnetic parameters given in Table I.

Hyperfine coupling constants were determined for ZnP with the MELDF (Ref. 48) suite of programs using singles and doubles configuration interaction (SDCI) from the single determinantal Hartree-Fock (HF) function and MRSDCI level of theory. The uncontracted Wachters[46] basis set with the recommended two additional p functions for zinc (14s 11p 5d) and an uncontracted Dunning[49] basis set with an additional p and d functions for phosphorus (11s 8p 1d) were used. Calculations were performed at the optimized geometry from the MCSCF calculations. The SDCI calculations included all single excitations from the HF configuration and those double excitations with a threshold energy exceeding 1×10^{-7} hartree. The MRSDCI calculations were performed in the same manner, except 100 reference configurations were chosen on the basis of their configuraton interaction (CI) coefficient in the SDCI calculation. All calculations were performed on a DEC Alpha DS10 workstation.

III. RESULTS

A. Neon matrices

Natural zinc metal consists of five isotopes and of these only ^{67}Zn has a nonzero nuclear spin ($I=5/2$, $\mu=0.875\ 24$) giving rise to a hyperfine interaction. The ESR signals arising from those isotopes with $I=0$ have been designated Zn for convenience with no specific isotopic label. Phosphorus has only one isotope, ^{31}P ($I=1/2$, $\mu=1.1317$) and for simplicity the signals arising from this species have been labeled P.

The ESR peaks assigned to the ZnP radical formed through the ablation of a zinc metal target with gallium phosphide powder pressed into the metal surface and then isolated in a neon matrix at 4.3 K are shown in Fig. 1. We observe the xy_1, xy_3 perpendicular peaks as well as an off-angle (OA) peak. The spectra were recorded at 4.3 K after annealing to 9.3 K, with a 20 mW microwave power and at a frequency for the xy_1, xy_3, and OA lines of 9715.864 MHz, 9708.799 MHz, and 9715.701 MHz, respectively. All peaks are split into 1:1 doublets from coupling to one phosphorus

TABLE I. Observed ESR line positions (gauss) for the perpendicular transitions of the ZnP radical.

ZnP			
Frequency (MHz)	M_I [a]	Obs.[b]	Calc.[c]
9715.864	1/2	1725.0(3)	1725.0
	−1/2	1764.5(3)	1764.7
9708.799[d]	1/2	11 614(1)	11 614
	−1/2	11 654(1)	11 653
9715.701	1/2	12 873(1)	12 873
	−1/2	12 885(1)	12 885
^{67}ZnP			
M_I[e]	M_I[a]	Obs.[b]	Calc.[c]
−5/2	1/2	1579.5(7)	1579.7
	−1/2	1619.4(7)	1619.5
−3/2	1/2	1634.7(7)	1634.6
	−1/2	1674.0(7)	1674.4
−1/2	1/2	1690.5(7)	1690.7
	−1/2	...[f]	1730.6
1/2	1/2	...[f]	1747.7
	−1/2	1787.5(7)	1788.0
3/2	1/2	1806.5(7)	1806.8
	−1/2	1845.8(7)	1846.2
5/2	1/2	1866.0(7)	1865.9
	−1/2	1905.9(7)	1905.7

[a]The magnetic quantum number for the ^{31}P (I=1/2) nucleus.
[b]Peak positions were measured from the apex of the peak; radical was in a neon matrix which had been annealed to 9 K then cooled to 4.3 K. Experimental uncertainty in the line positions was ±0.2–0.3 G. The microwave frequency was 9714.370 MHz for ^{67}ZnP.
[c]The calculated line positions were determined by exact diagonalization using the magnetic parameters listed in Table II.
[d]A second site was observed for the xy_3 peaks at 11 634(1) and 11 675(1) G.
[e]The magnetic quantum number for the ^{67}Zn (I=5/2) nucleus.
[f]Two ^{67}ZnP hyperfine peaks were obscured by the ZnP xy_1 peaks.

nucleus (I=1/2). The hyperfine splitting observed for the OA doublet peaks is significantly smaller than that of the perpendicular doublets. The xy_3 lines show an additional splitting, attributed to the ZnP radicals occupying two slightly different sites in the neon matrix. The parallel peaks are expected to be considerably weaker than the perpendicular lines and were not observed. The xy_1 doublet was the most intense and was found at magnetic fields indicative of a $^4\Sigma$ state.[50] The perpendicular line positions for the radical are given in Table I.

The magnetic hyperfine parameters for ZnP were obtained by fitting the simulated line positions (Fig. 1) obtained by exact diagonalization of the spin Hamiltonian with the experimental peak positions within their experimental uncertainty. The parameters obtained are given in Table II and assume axial symmetry with a $^4\Sigma$ electronic ground state. The simulated peaks gave a good match for peak position, line shape, and peak intensity when compared with the experimental peaks. The position of the OA peaks was sensitive to the parallel hyperfine magnetic parameters allowing reasonable estimates to be made for $g_\parallel$ and $A_\parallel$ even though parallel features were not observed. The signs obtained for the hyperfine coupling constants were not obtained experimentally and were based on the theoretical predictions. Each of the xy_3 doublets had slightly different magnetic parameters, and was simulated separately, then the two were summed to produce the resultant spectrum shown in the upper trace of Fig. 1. The ratio of the sites was approximately 1:1. For a radical with a $^4\Sigma$ ground state four transitions are possible: xy_1, xy_2, xy_3, and z.[50,51] Only two transitions were observed for the ZnP radical, as the z peaks were too weak to be seen and the xy_2 transition could not be seen as a result of the large zero-field splitting, D.[50,51] The observed transitions can be more easily seen by superimposing the simulated ZnP spectrum with the corresponding θ versus B plot (supplementary material).[52] The large D value has little effect on the position of the xy_1. This insensitivity meant that the overall fit of the magnetic parameter is more dependent on the position of the xy_3 and OA peaks, rather than the position of the xy_1 doublet.

The assignment of the xy_1 doublet pattern resulting from ZnP was also supported by the detection of the ^{67}ZnP radical. The ^{67}ZnP radical spectrum (Fig. 2) was recorded at 4.3 K with a 10 mW microwave power and at a frequency of 9714.37 MHz. The perpendicular line positions for the radical are given in Table I. The spectrum of the ^{67}ZnP is expected to consist of six widely spaced doublets. The spacing in each doublet of the ^{67}Zn hyperfine transitions is the same as the doublet spacing for ZnP radical. The natural abundance of ^{67}Zn is 4.1%, thus the intensity of each of the sextet components should be about 0.7% of the original ZnP peak intensity. The spectrum consists of a sextet of doublets at the expected spacing and intensity. Due to the overlap of the xy_1 line from ZnP the higher field peak of the $m_I=-1/2$ doublet and the lower field peak of the $m_I=1/2$ doublet could not be

TABLE II. Magnetic parameters (megahertz) for the ZnP radical trapped in a neon matrix at 4.3 K.

	$g_\perp$	$g_\parallel$	$A_\perp$	$A_\parallel$	A_{iso}[a]
P (site 1)	1.9982(2)	1.9941(2)	111(6)	−5(6)	72(9)
P (site 2)	1.9982(2)	2.0001(2)	111(6)	−5(6)	72(9)
^{67}Zn	1.9982(2)	1.9941(2)	160(2)	180(50)	167(30)
	A_{dip}[a]	$D_{x,y}$	D_z		D
P (site 1)	−39(15)	−9996(1)	19 992(2)		−29 988(3)
P (site 2)	−39(15)	−10 028(1)	20 057(2)		−30 085(3)
^{67}Zn	6(4)	−9996(1)	19 992(2)		−29 988(3)

[a]A_{iso} and A_{dip} were calculated from standard equations (Ref. 50) which neglected **L•S** effects. Experimental work cannot determine the sign of A_{iso} or A_{dip}; therefore, the signs are based on the theoretical values.

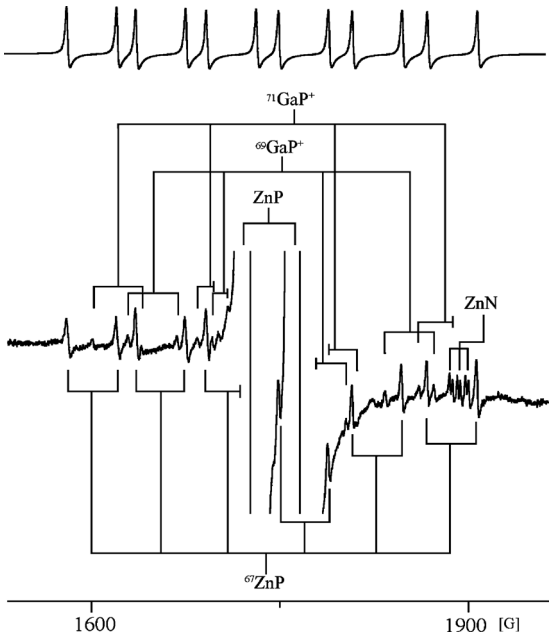

FIG. 2. The lower trace shows the ESR spectrum for the ^{67}ZnP radical isolated in a neon matrix at 4.3 K. Multiple spectra were recorded with a 10 mW microwave power and at a frequency of 9714.37 MHz. Transitions from impurities $^{69/71}$GaP$^+$ and ZnN are also observed. The upper trace shows the simulated ESR spectrum for the ^{67}ZnP radical obtained using the magnetic parameters given in Table I.

resolved. Impurity peaks due to $^{69/74}$GaP$^+$ (Ref. 53) were also observed, presumably a result of the gallium phosphide starting material. Although in the same region as the peaks of interest, the yield of the $^{69/71}$GaP$^+$ was significantly less than that of ^{67}ZnP and thus did not interfere with analysis. The simulated ESR spectrum of ^{67}ZnP radical is also contained in Fig. 2. The magnetic hyperfine parameters obtained for the Zn-67 nucleus are shown in Table II, the signs obtained for the hyperfine coupling were based on theoretical predictions.

The ESR xy_1 transition assigned to the MgP radical is shown in Fig. 3. The spectrum was recorded at 4.3 K, with a 5 mW microwave power and at a frequency of 9715.636 MHz. The radical was formed by the ablation of a magnesium metal target with gallium phosphide powder pressed into the metal surface and then isolated in a neon matrix at 4.3 K. Analogous to the ZnP experiments, the phosphorus nucleus should split the observed signal into a 1:1 doublet. The xy_1 observed is not exactly 1:1 as a ^{69}GaP$^+$ peak overlaps with the higher field xy_1 peak. Only the xy_1 perpendicular doublet with an $A_\perp$ of 157(6) MHz was observed due to the extremely low yield of MgP. The xy_1 doublet was found at a magnetic field that is indicative of a $^4\Sigma$ state.[50] The low yield is emphasized in Fig. 3, the observed xy_1 is only twice as intense as those assigned to the $^{69/71}$GaP$^+$ radicals. These peaks were only about one-third as intense as the ^{67}ZnP xy_1 peaks. Subsequent experiments to improve the yield of MgP were hindered by the formation of CdP due to the presence of background cadmium metal in the system from subsequent experiments.

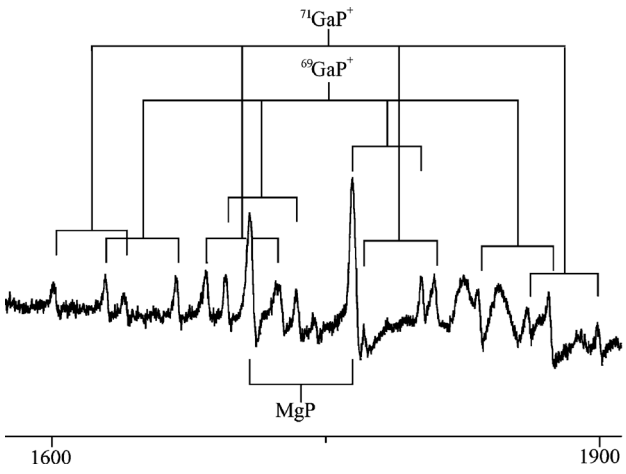

FIG. 3. The ESR xy_1 transition assigned to MgP radical isolated in a neon matrix at 4.3 K, with a 5 mW microwave power and at a frequency of 9715.636 MHz. Transitions assigned to the $^{69/71}$GaP$^+$ radicals are also evident.

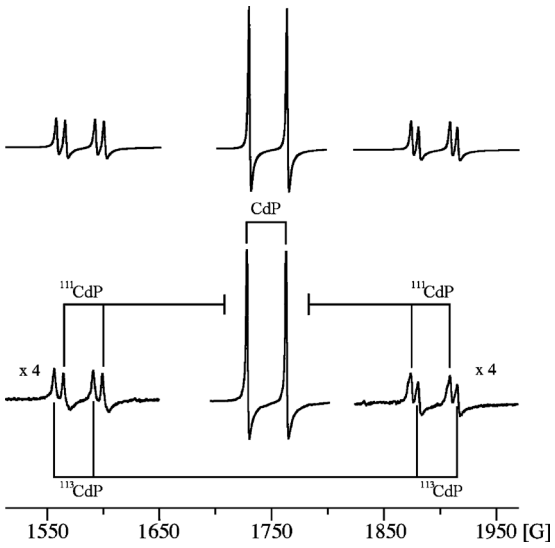

FIG. 4. The lower trace shows the xy_1 transition assigned to the CdP and $^{111/113}$CdP radicals isolated in a neon matrix at 4.3 K. The spectra were recorded with a 30 mW microwave power and a frequency of 9710.611 MHz for CdP and 9711.566 MHz for $^{111/113}$CdP. The upper trace shows the simulated ESR spectrum for the CdP and the $^{111/113}$CdP radicals obtained using the magnetic parameters in Table III.

Natural cadmium metal consists of eight isotopes. Of these, ^{111}Cd (I=1/2, μ=−0.594 28, abundance 12.75%) and ^{113}Cd (I=1/2, μ=−0.621 67, abundance 12.26%) have a nonzero nuclear spin. The ESR signals arising from those isotopes with I=0 will be designated Cd for convenience with no specific isotopic label. The ESR xy_1 transitions assigned to the CdP and the $^{111/113}$CdP radicals are shown in Fig. 4. The line positions for the radicals are contained in Table III. The spectra were recorded at 4.3 K, with a 30 mW microwave power and at a frequency of 9710.611 MHz for CdP and 9711.566 MHz for $^{111/113}$CdP. The radicals were formed by the ablation of a cadmium metal target with gallium phosphide powder pressed into the metal surface and then isolated in a neon matrix at 4.3 K. As in the previous two cases the phosphorus nucleus splits the signal into a 1:1 doublet. Even though the CdP yield was higher than that of ZnP, only the xy_1 transition was observed. This is thought to be due to the other CdP lines occurring at higher fields than those able to be measured by the experimental equipment

TABLE III. Observed ESR line positions (gauss) for the perpendicular transitions of the CdP, ^{111}CdP, and ^{113}CdP radicals.

CdP			
M_I [a]	Obs.[b]	Calc.[c]	
1/2	1729.3(3)	1729.2	
−1/2	1764.2(3)	1764.2	
^{111}CdP			
M_I [d]	M_I [a]	Obs.[b]	Calc.[c]
1/2	1/2	1565.7(5)	1565.6
1/2	−1/2	1600.1(5)	1599.9
−1/2	1/2	1875.2(5)	1875.1
−1/2	−1/2	1910.3(5)	1910.8
^{113}CdP			
M_I [d]	M_I [a]	Obs.[b]	Calc.[c]
1/2	1/2	1557.1(5)	1557.0
1/2	−1/2	1592.3(5)	1592.1
−1/2	1/2	1887.8(5)	1882.2
−1/2	−1/2	1916.9(5)	1916.5

[a]The magnetic quantum number for ^{31}P (I=1/2) nucleus.
[b]Peak positions were measured from the apex of the peak; the radical was in a neon matrix at 4.3 K. The experimental uncertainty in the line positions was ±0.2–0.3 G.
[c]Parameters listed in Table IV were used in the diagonalization of the spin Hamiltonian to obtain these values. The microwave frequency was 9715.802 MHz for CdP and 9715.650 MHz for $^{111/113}$CdP.
[d]The magnetic quantum number for $^{111/113}$Cd (I=1/2) nucleus.

and will be discussed later. The parallel peaks were considerably weaker than the perpendicular peaks and were not observed. The xy_1 doublet was found at similar magnetic fields to the two previously discussed phosphides and implies a $^4\Sigma$ ground state. The result was supported by the simulation of the spectra (Fig. 4). The $^{111/113}$Cd hyperfine transitions consist of a pair of doublets (one pair for each isotope) with the spacing within each doublet equal to the CdP doublet spacing. The intensities of ^{111}CdP and ^{113}CdP radical peaks were 6.4% and 6.1%, which are consistent with the intensities predicted based on natural abundances of the isotopes. This higher intensity makes these lines relatively easy to find in comparison to those of the ^{67}ZnP radical.

The magnetic hyperfine parameters for CdP and $^{111/113}$CdP are given in Table IV and were obtained analogously to the ZnP parameters. The set of parameters obtained assumed axial symmetry and a $^4\Sigma$ electronic ground state. As

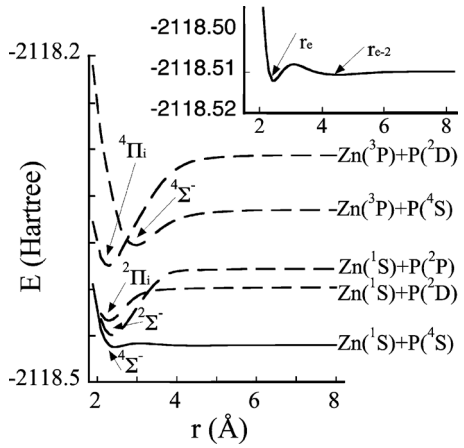

FIG. 5. The potential energy surfaces for the low-lying electronic states of ZnP. The active space used in the calculation consisted of seven electrons and eight orbitals. The resulting binding energies, energy separations, and leading configurations for the electronic states are shown in Table V. The inset shows an expanded form of the ground $^4\Sigma^-$ state, highlighting the second shallow minima (r_{e-2}).

only the xy_1 was observed, the D value for the ZnP radical was used in the simulation. This D value would be smaller than the actual value due to the larger atomic number of the cadmium nucleus compared with the zinc nucleus. The peaks obtained from the magnetic parameters were a good match for line position, line shape, and peak intensity to the experimental peaks. The $g_\parallel$ and $A_\parallel$ values could not be determined due to a lack of parallel features and the insensitivity of the perpendicular peaks to these parameters. The signs obtained for the hyperfine coupling constants cannot be obtained experimentally and were based on theoretical predictions.

B. Theoretical

Figure 5 shows the calculated potential energy surfaces (PES) for the five lowest-lying independent electronic states of ZnP. In total, seven states were calculated, but both the $^2\Pi_i$ and $^4\Pi_i$ correspond to degenerate spin states. For each of the states, energy as a function of bond distance between the zinc and phosphorus atoms is shown. Table V contains the leading configurations, binding energies $-D_e$, and energy separations T_e for each of the states in ascending energy order at the optimized geometry. The full configuration of the radical is $1\sigma^2 2\sigma^2 3\sigma^2 4\sigma^2 5\sigma^2 1\pi^4 6\sigma^2 2\pi^4 7\sigma^2 8\sigma^2 3\pi^4 9\sigma^2 4\pi^4 1\delta^4 10\sigma^2 11\sigma^2 5\pi^2 12\sigma^1$. For simplicity, the leading configurations do not include the core orbitals nor the zinc 3d electrons, as for zinc the bonding is expected to occur when one

TABLE IV. Magnetic parameters (megahertz) for the CdP radical trapped in a neon matrix at 4.3 K.

	$g_\perp$ [a]	$A_\perp$ [b]	$D_{x,y}$ [c]	D_z [c]	D[c]
P	1.9963(2)	97(3)	−9996	19 992	−29 988
^{111}Cd	1.9963(2)	862(3)	−9996	19 992	−29 988
^{113}Cd	1.9963(2)	902(3)	−9996	19 992	−29 988

[a]$g_\parallel$ is assumed equal to g_e.
[b]$A_\parallel$ is assumed equal to $A_\perp$ as no parallel lines or OA peaks, which could be used to determine the values, were observed.
[c]$D_{x,y,z}$ and D values are given as a lower limit to actual values as no parallel lines or OA peaks, which could be used to determine the values, were observed.

TABLE V. Leading configurations, binding energies ($-D_e$), and energy separations (T_e) for the electronic states of ZnP.

State	r_e (Å)	$-D_e$ (kJ/mol)	T_e (eV)[a]	Configuration[b]	Leading (%)
$^4\Sigma^-$	2.450	6.011	0[c]	$10\sigma^2 11\sigma^2 5\pi^1 5\pi^1 12\sigma^1$	94.7
	4.540	1.921	0.042	$10\sigma^2 11\sigma^2 5\pi^1 5\pi^1 12\sigma^1$	42.0
$^2\Sigma^-$	2.381	186.3	0.349	$10\sigma^2 11\sigma^2 5\pi^1 5\pi^1 12\sigma^1$	43.3
$^2\Pi_i$	2.294	93.40	0.772	$10\sigma^2 11\sigma^2 5\pi^1 5\pi^2$ [d]	81.2
$^2\Pi_i$	2.294	93.40	0.772	$10\sigma^2 11\sigma^2 5\pi^2 5\pi^1$ [d]	81.4
$^4\Pi_i$	2.293	310.2	2.376	$10\sigma^2 11\sigma^1 5\pi^1 5\pi^2 12\sigma^1$ [d]	96.0
$^4\Pi_i$	2.293	310.2	2.376	$10\sigma^2 11\sigma^1 5\pi^2 5\pi^1 12\sigma^1$ [d]	96.0
$^4\Sigma^-$	2.981	98.63	2.975	$10\sigma^2 11\sigma^1 5\pi^1 5\pi^1 12\sigma^2$	61.2

[a]Theoretical values calculated with MCSCF(7,8) using a TZV basis with additional p, d, and f functions on both zinc and phosphorus.
[b]Configurations were taken at r_e for each state. For ease the core and 3d orbitals have been omitted.
[c]Actual energy calculated for $^4\Sigma^-$ was −2118.512 hartree. This value was set to 0 eV and all other states have been referenced to this state.
[d]Two leading configurations with approximately the same weighting exist and have been summed as they only differ in placement of the spin up or spin down electron in the π_x and π_y orbitals.

of the $4s^2$ electrons is promoted to a 4p or dative bonding occurs.[18] The ground state calculated for a $^4\Sigma^-$ and has a zinc-phosphorus bond length r_e of 2.450 Å, total energy E of −2118.512 hartree, and $-D_e$ of 6.011 kJ/mol. The ZnP radical dissociates into zinc (^{1}S) and phosphorus (^{4}S) atoms. A second very shallow minimum with an energy of −2118.511 hartree at 4.540 Å and $-D_e$ of 1.921 kJ/mol also exists. The atomic dissociation products for each ZnP state are given on each PES in Fig. 5. A comparison of the calculated dissociation energies for each of the electronic states with those obtained experimentally[54–56] is contained in the supplementary material.[52] The magnetic parameters for ZnP were also calculated and are compared with the experimentally derived values shown in Table VI.

The PESs for the low-lying electronic states of MgP are given in Fig. 6. Analogous to the ZnP calculations, both the $^2\Pi_i$ and $^4\Pi_i$ comprised of degenerate spin states. Energy as a function of bond distance between the magnesium and phosphorus atoms is shown for each of the states. Table VII shows the leading configurations, $-D_e$ and T_e, for each state in ascending energy order at the optimized geometry. The full configuration of the radical is $1\sigma^2 2\sigma^2 3\sigma^2 4\sigma^2 5\sigma^2 1\pi^4 6\sigma^2 2\pi^4 7\sigma^2 8\sigma^2 3\pi^4 9\sigma^1$. For simplicity, the leading configurations do not include the core orbitals. The calculated ground state of the MgP radical is a $^4\Sigma^-$ state, with a magnesium-phosphorus r_e of 2.512 Å, E of −540.363 hartree, and $-D_e$ of 24.47 kJ/mol. The radical dissociates into magnesium (^{1}S) and phosphorus (^{4}S) atoms. The magnesium and phosphorus dissociated states for each of the PESs are shown in Fig. 6. A comparison of these with experimentally derived values[54–56] can be found in the supplementary material.[52]

TABLE VI. Comparison of experimental and theoretical hyperfine coupling constants (megahertz) of ZnP radical.

		A_{iso}	A_{dip}
B3PW91	P	−52.952	−142.020
	^{67}Zn	147.635	12.289
B3LYP	P	−18.313	−127.551
	^{67}Zn	139.396	11.603
Full MP2[a]	P	−30.360	−124.643
	^{67}Zn	109.407	10.348
SDCI[a,b]	P	−31.355	−64.853
	^{67}Zn	184.105	4.207
MRSDCI[a,c]	P	−19.804	−63.287
	^{67}Zn	180.708	4.111
Expt.	P	72(9)	−39(15)
	^{67}Zn	167(30)	6(4)

[a]Basis sets. For zinc, uncontracted Wachters (Ref. 46) with two additional recommended p functions (14s 11p 5d). For phosphorus, uncontracted Dunning double zeta plus polarization (DZP) with additional p and d functions (11s 8p 1d) (Ref. 47).
[b]All single excitations from the HF configuration and those double excitations with a threshold energy exceeding 1×10^{-7} hartree were used in the CI.
[c]100 reference configurations chosen from the SDCI coefficients.

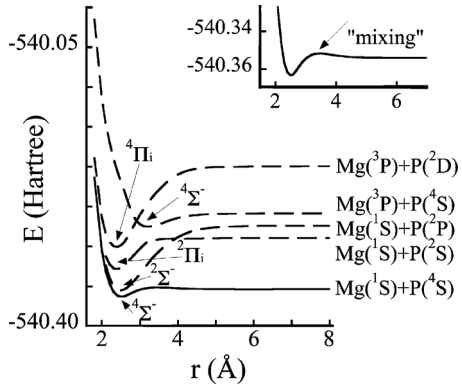

FIG. 6. The potential energy surfaces for the low-lying electronic states of MgP. The active space used in the calculation consisted of seven electrons and eight orbitals. The resulting binding energies, energy separations, and leading configurations for the electronic states are shown in Table VII. The inset shows an expanded form of the ground $^4\Sigma^-$ state, highlighting the bump resulting from mixing between the ground and excited $^4\Sigma^-$ states.

TABLE VII. Leading configurations, binding energies ($-D_e$), and energy separations (T_e) for the electronic states of MgP.

State	r_e (Å)	$-D_e$ (kJ/mol)	T_e (eV)[a]	Configuration[b]	Leading (%)
$^4\Sigma^-$	2.512	24.47	0[c]	$7\sigma^2 8\sigma^2 3\pi^1 3\pi^1 9\sigma^1$	95.6
$^2\Sigma^-$	2.487	205.2	0.214	$7\sigma^2 8\sigma^2 3\pi^1 3\pi^1 9\sigma^1$	40.5
$^2\Pi_i$	2.380	102.8	0.939	$7\sigma^2 8\sigma^2 3\pi^1 3\pi^2$ [d]	73.4
$^2\Pi_i$	2.380	102.8	0.939	$7\sigma^2 8\sigma^2 3\pi^2 3\pi^1$ [d]	73.6
$^4\Pi_i$	2.375	265.8	1.701	$7\sigma^2 8\sigma^1 3\pi^1 3\pi^2 9\sigma^1$ [d]	96.1
$^4\Pi_i$	2.375	265.8	1.701	$7\sigma^2 8\sigma^1 3\pi^2 3\pi^1 9\sigma^1$ [d]	96.1
$^4\Sigma^-$	3.215	43.86	2.392	$7\sigma^2 8\sigma^1 3\pi^1 3\pi^1 9\sigma^2$	42.1

[a]Theoretical values calculated with MCSCF(7,8) using cc-pVDZ basis on both magnesium and phosphorus.
[b]Configurations were taken at r_e for each state. For ease the core orbitals have been omitted.
[c]Actual energy calculated for $^4\Sigma^-$ was −540.363 hartree. This value was set to 0 eV and all other states have been referenced to this state.
[d]Two leading configurations with approximately the same weighting exist and have been summed as they only differ in placement of the spin up or spin down electron in the π_x and π_y orbitals.

IV. DISCUSSION

A. Formation and comparison of metal phosphide radicals

The formation of radicals in this work involved ablating a metal target into which crushed gallium phosphide crystals had been pressed. This varied to other work carried out in this laboratory, whereby reactant gas mixtures are introduced into the deposition chamber either in pure or dilute form from a capillary located directly below the metal target.[13–15] Initial attempts to form ZnP and ^{67}ZnP involved the injection of PH_3/neon gas mixtures into the deposition chamber containing a zinc metal target, which was ablated. This resulted in the formation of ZnP in relatively low yields with the ESR signal being 20 times less intense than those obtained using gallium phosphide crystals. The low yield resulted in only the ZnP xy_1 line being observed. In addition, no transitions attributable to the ^{67}ZnP radical were observed. A comparison of the xy_1 transitions measured from both experimental techniques is contained in the supplementary material.[52]

The assignment of peaks to the ZnP radical was slightly unusual as the OA lines occurred at higher field than the xy_3 lines. An alternate fit with magnetic parameters that reversed the assignment of the xy_3 and OA lines was not possible. Simulations fitting the OA lines at 11 614 and 11 654 G placed the xy_3 lines at around 10 750 and 10 780 G. No experimental evidence of peaks at this field was found. Further evidence justifying the assignment of the peaks to the ZnP radical include the fact that none of the peaks photobleached, all peaks displayed a similar power dependence, and finally the intensities of all peaks had a similar temperature dependence. The smaller splitting exhibited by the higher field doublet attributed to the OA feature was replicated in the simulation.

Figure 7 shows a comparison of the xy_1 transitions of the MgP, ZnP, and CdP radicals. All species have a $^4\Sigma$ ground state and although they are found at approximately the same field, the $A_\perp$ values for each species were quite different. As the size of the metal atom increased, the splitting between the phosphorus doublet and therefore the $|A_\perp|$ value decreased. The value of the phosphorus $A_\perp$ observed was 157 MHz for the MgP radical, 111 MHz for the ZnP radical, and 97 MHz for the CdP radical. The similarities between the $A_\perp$ values of the ZnP and CdP radicals compared to the much larger value obtained for the MgP radical may be associated with the charge density on the phosphorus atom. For the larger metal nuclei more of the electron density can be located on the phosphorus atom resulting in smaller $A_\perp$ values representative of the stronger coupling.

The xy_1 transitions for each of the radicals formed all occur at very similar fields. This can be explained by the species having large D parameters associated with them. The $|D|$ calculated for ZnP is large (29 988 MHz). In a $^4\Sigma$ radical the position of the xy_1 peak will be relatively constant at high values of D, thus the xy_1 peak positions are more dependent on the g value.[50] A large D parameter has been seen in other $^4\Sigma$ radicals comprised of heavier elements, Ga_2^-

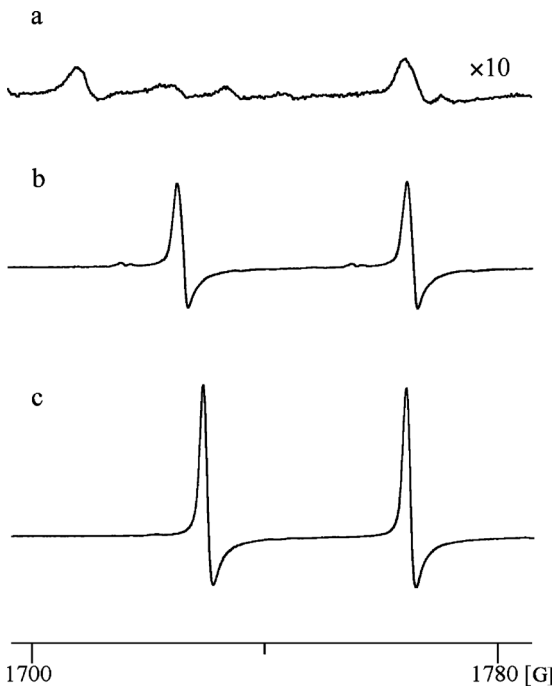

FIG. 7. A comparison of the xy_1 transitions observed for the (a) MgP, (b) ZnP, and (c) CdP radicals.

(Ref. 57), while lighter $^4\Sigma$ radicals like Al_2^- tend to have smaller D parameters.[57] The value of the D parameter is made up of two contributions: D_{SO} arising from spin orbit coupling and D_{SS} spin-spin interaction. D_{SO} is proportional to the atomic number of the nuclei in the radical, resulting in larger D and smaller $g_\perp$ parameters for radicals with heavier nuclei. The values for the spin orbit coupling constants for Zn and Cd are 386 cm^{-1} and 1141 cm^{-1}, respectively.[58] These are large compared to the lighter Mg nuclei, 41 cm^{-1}.[58] Thus, it is reasonable for the D parameter to be larger for heavier systems. In addition, a decrease in $g_\perp$ was observed with increase in mass. ZnP radical $g_\perp$ is 1.9982 compared with 1.9963 for CdP.

Although relatively large yields of the CdP radical (cf. ZnP) were achieved, there was no evidence of an xy_3 or OA peak in the spectrum. This is likely the result of the D value for the CdP radical being larger than that of the ZnP radical. The high field lines of the ZnP radical were at the upper field limit of the instrumentation, thus making it likely that the xy_3 and OA peaks of the CdP radical are not in the instrumentation field range. This result has been seen previously in the Al_2^- experiments.[57] The simulated spectrum for the CdP radical used the D values from the ZnP radical as a minimum for the actual value.

The low yields attained for the MgP radical compared to those of ZnP were unexpected as theory suggested that the ground state has a larger dissociation energy than the ZnP radical. However, theory can only predict the stability of a species once formed, indicating that the low yields are most likely due to the alternate gas phase reactions and kinetics in the ZnP and CdP cases.

B. Comparison between theoretical and experimental hyperfine coupling constants

Table VI provides a comparison between theoretical A_{iso} and A_{dip} values and those found experimentally. Overall the theoretical methods gave a reasonable fit for the ^{67}Zn values but a poor fit for P values. The inability of the theory to provide an adequate fit for the hyperfine coupling constants of the substituent to the metal is analogous to findings for the CH_3Cd and CH_3Zn radicals.[13,14] The value of $A_{iso}(^{67}Zn)$ obtained for all levels of theory was within the experimental uncertainty apart from full MP2, which was 20% below the experimental uncertainty. Theory generally predicts $A_{dip}(^{67}Zn)$ to be small as was found experimentally. MRSDCI and SDCI gave the closest estimates.

Feller[59] noted that the hyperfine parameters are particularly sensitive to the basis set used. Calculation of spin properties depends on both core/valence recovery as well as geometry. The optimized geometry used in this calculation should be sufficient to ensure that calculated values are in the frame of the nuclei. It is more likely that the discrepancy arises from the inability of the basis set to model the nucleus effectively, resulting in the over- or underestimating of the hyperfine coupling constants.[59]

C. Bonding and electronic structure

A free atom comparison method (FACM) analysis was carried out for the ZnP radical. The procedures and equations employed for the $^4\Sigma$ ZnP radical were the same as those used for the $^4\Sigma$ BC radical.[60] The FACM involves taking the ratio of the experimentally determined molecular A_{iso} and A_{dip} with the free atomic A_{iso} and A_{dip} for each nuclei in the radical. This method allows an evaluation of the contribution from each atomic orbital (AO) in the molecular orbitals (MOs) of the radical. The FACM is an approximation and does not account for hyperfine contributions from orbitals on other atoms, overlap effects, or core polarization. For the ZnP radical, it is expected that two of the electrons will be localized on the phosphorus atom, in π type orbitals, and the third electron would be in a σ type on the zinc. The MOs are expected to have the following AO occupancies:

$$\sigma = a_1\chi(\mathrm{Zn}\ \ 4s) + a_2\chi(\mathrm{Zn}\ \ 4p_z) + a_5\chi(\mathrm{P}\ \ 3s) + a_6\chi(\mathrm{P}\ \ 3p_z),$$

$$\pi_x = a_3\chi(\mathrm{Zn}\ \ 4p_x) + a_7\chi(\mathrm{P}\ \ 3p_x),$$

$$\pi_y = a_4\chi(\mathrm{Zn}\ \ 4p_y) + a_8\chi(\mathrm{P}\ \ 3p_y),$$

where χ represents the atomic orbitals and a_i, the spin densities give the coefficient of each AO in the MO. The a_i values can be determined using FACM, but some assumptions need to be made. The perpendicular x and y directions of the ZnP radical are equivalent; therefore, $a_3=a_4$ and $a_7=a_8$. The π type orbitals are assumed to be totally phosphorus $3p_x$ and $3p_y$, i.e., $a_7=a_8=0.333$. Thus a_3 and a_4 are assumed to be zero even though they would be expected to have a small contribution to the MO composition. The following equations and relationships were used for the analysis:

$$a_1 = A_{iso}(\mathrm{molecule})/A_{iso}(\mathrm{atom}),$$

$$a_5 = A_{iso}(\mathrm{molecule})/A_{iso}(\mathrm{atom}),$$

$$0.333 = a_1 + a_2 + a_5 + a_6,$$

$$a_6 - 0.333 = A_{dip}(\mathrm{molecule})/A_{dip}(\mathrm{atom}).$$

The values obtained for this and the Mulliken spin population analysis from MRSDCI are given in Table VIII. The experimental values show some zinc 4s, almost no phosphorus 3s, and the phosphorus $3p_z$ contribution is overestimated. The zinc $4p_z$ character in all likelihood is showing up as an increase in the phosphorus $3p_z$ character. The 4s zinc character is substantially lower than that predicted by the Mulliken spin population. This could be due to pairing of electrons in the zinc $4p_z$ orbital. This would lower the unpaired electron spin density of the zinc $4p_z$ as observed. The FACM method is severely limited due to the approximations made. This accounts for the difference in the experimental and Mulliken spin populations. It should be noted that in previous theoretical studies[13–15] by this group, it has been found that there is some uncertainty in the Mulliken spin populations due to the CI not weighting the various configurations correctly.

TABLE VIII. Comparison of the experimental and theoretical spin densities for the ZnP radical.

	^{67}Zn				P				Total
	$a_1^2\chi(4s)$	$a_2^2\chi(4p_x)$	$a_3^2\chi(4p_y)$	$a_4^2\chi(4p_z)$	$a_5^2\chi(3s)$	$a_6^2\chi(3p_x)$	$a_7^2\chi(3p_y)$	$a_8^2\chi(3p_z)$	$\Sigma_{i=1}^{8}a_i^2$
^{67}ZnP [a]	0.084(2)	0[b]	0[b]	0.017(1)	0.0054(7)	0.33[c]	0.33[c]	0.23(9)	1.0
MRSDCI[d]	0.16	0.012	0.012	0.065	0.0068	0.32	0.32	0.095	0.99

[a]The experimental values are calculated using the free atom comparison method (see text). The indicated uncertainties reflect only the experimental uncertainties in A_{iso} and A_{dip}.
[b]These were assumed to be zero (see text).
[c]These were assumed to be 0.33 (see text).
[d]Gross spin populations from the MRSDCI calculation with 100 reference configurations and a threshold for retaining double excitations in the CI of 1×10^{-7} hartree.

D. Theoretical results, MgP

The r_e obtained for the $^4\Sigma^-$ and $^2\Pi$ are similar to the values obtained by Boldyrev and Simons.[17] Similar energetics were also obtained at r_e in comparison to Boldyrev and Simons' work, with the leading configurations for the $^4\Sigma^-$ and $^2\Pi$ being the same.[17]

For MgP, restricted open shell Hartree-Fock (ROHF) calculations were performed at an r close to r_e and the vectors generated were then used as an initial guess for the MCSCF calculation. Both the natural and MCSCF orbitals were generated from the calculation and either set could be used as a guess for the vectors at the next r, since both give the same result. The excited $^4\Sigma^-$ state was found to lie only 2.392 eV higher than the ground $^4\Sigma^-$ state. This was close enough to lead to significant mixing between the states, namely, 27.3% of the excited state consisted of the ground electronic configuration and 21.0% of the ground state consisted of the excited configuration. This interaction can be seen as a small "bump" (inset of Fig. 6) in the ground state at $r\approx r_e$ of the excited state.

Calculations for the doublet systems were much more difficult to perform. At $r\approx3.9$ Å the PES for the $^2\Sigma^-$ state crosses the two degenerate $^2\Pi$ PESs. At r=3.9 Å the second order MCSCF would not converge for all states as the Hessian contained a large number of negative eigenvalues. At $r>3.9$ Å all states converged to dissociation energy higher than those for calculations performed at $r<3.9$ Å. Initial attempts to rectify this problem involved changing the second order approximation to an exact orbital Hessian from an approximate Hessian, using smaller r increments in conjunction with ROHF, natural and MCSCF orbitals as guesses for each calculation, obtaining starting vectors at 3.8 and 3.9 Å from a configuration interaction single and double excitations (CISD) calculation and use of a smaller active space as a guess for the next calculation, which was performed with a slightly larger active space, and then slowly building up to the full active space was also attempted. The failure of all of the aforementioned techniques was due to the optimization of the MOs of one of the degenerate $^2\Pi$ rather than the $^2\Sigma^-$. Maintaining the optimization of the $^2\Sigma^-$ MOs solved this.

E. Theoretical results, ZnP

The r_e obtained for the $^4\Sigma^-$ and the occurrence of both short and long minima was in agreement with all but the B3LYP results seen by Boldyrev and Simons,[18] with the values for the $^2\Pi$ and the leading configurations for both also in agreement. The energetics of this work suggest that the bond strength of both states is slightly weaker (~0.3 hartree) than Boldyrev and Simons' results.

Unlike MgP, the choice of MOs used for a guess was critical. When ROHF or natural MOs were used, the calculation predicted an unbound $^4\Sigma^-$ ground state. It was only when MCSCF MOs from the previous calculation were used that a bound $^4\Sigma^-$ ground state was predicted. The excited $^4\Sigma^-$ state was 2.975 eV higher than the ground $^4\Sigma^-$ state. This results in significantly less mixing (approximately half) than that seen for MgP. The absence of a bump in the PES of the ground quartet state at $r\approx r_e$ of the excited state was the result of less mixing between the two.

A qualitative MO diagram for the ground $^4\Sigma^-$ electronic state of ZnP is shown in Fig. 8. Both the major AO (coefficient >0.1) and minor AO contributions (coefficient <0.1) to each MO are shown. The AO separations are qualitative and are based on Slater's interpretation.[61] The singly occupied molecular orbitals are predominantly composed of the following atomic orbitals: $1\pi_{x,y}$-phosphorus $3p_{x,y}$; 3σ-zinc 4s, $4p_z$; and phosphorus $3p_z$. A large amount of density of the unpaired 3σ electron is located on the metal. This qualitative MO diagram also applies to MgP with the 3s and 3p AOs required for the metal atom.

Calculations for the doublet systems presented difficulties, the PES for the $^2\Sigma^-$ state crosses the degenerate $^2\Pi$ PESs at $r\approx3.4$ Å. Calculations at this point would not converge in the second order optimization. For calculations performed at $r>3.4$ Å the states converged to a dissociation

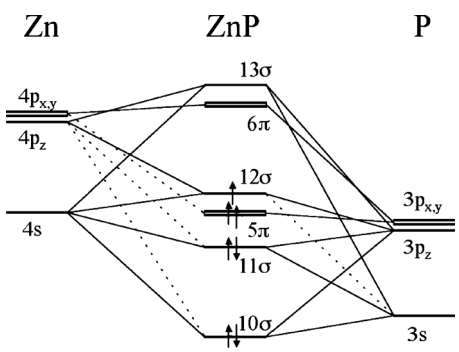

FIG. 8. A qualitative MO diagram for the ground $^4\Sigma^-$ state of the ZnP radical. The significant (coefficient >0.1) atomic orbital contributions are shown as solid lines with the minor contributions (coefficient <0.1) as dashed.

energy greater than that at $r < 3.4$ Å. The methods attempted above for MgP were employed for ZnP. However, none succeeded in maintaining the optimization of the $^2\Sigma$ MOs.

For excited states, state averaging is a recognized method used purely for attaining convergence of the MCSCF.[62] This technique involves optimizing the average energy of several electronic states.[63] In the case of ZnP, initially the lowest lying $^2\Sigma^-$ was optimized, then the MOs generated from this calculation were used as a guess for the next calculation. The state averaging method was only required for $r > 3.4$ Å, as at $r < 3.4$ Å MCSCF MOs from the previous calculation were sufficient as an initial guess. It should be noted that the degenerate $^2\Pi$ states only used three state averaging for the initial guess of the MOs, as this method had lower energetics than when the MOs are further optimized.

F. Comparison of MgP and ZnP

The PESs for both MgP and ZnP radicals exhibit very similar characteristics. In fact the only significant difference is the energy separation of the low-lying electronic states and the increase in mixing for MgP. This is most likely due to the energy difference of the valence AOs of zinc and magnesium. Species with low-lying electronic states (regardless of multiplicity) that couple strongly to the ground state have larger D_{SO} values. The greater the D_{SO} the larger the D value. A larger D_{SO} value for MgP would be expected compared to ZnP. However, this would probably be somewhat counterbalanced by the smaller atomic number.

The use of the MCSCF technique for both radicals is supported by the low leading coefficients obtained for all but the ground $^4\Sigma^-$ and $^4\Pi$ states at r_e. Leading coefficients for all states at r other than r_e generally show a reduction of the contribution of the HF configuration. For example, the ZnP ground $^4\Sigma^-$ state at 4.2 Å is only 44.6% $10\sigma^2 11\sigma^2 5\pi^1 5\pi^1 12\sigma^1$ as opposed to the 94.7% at r_e. To obtain accurate PESs MCSCF is essential as a dominant HF configuration is atypical.

V. SUMMARY

The ZnP, ^{67}ZnP, CdP, and $^{111/113}$CdP radicals were generated by the laser ablation of the metal target with gallium phosphide pressed into the metal surface. The radicals were then isolated in a neon matrix and their electronic structure probed using ESR spectroscopy. Pressing gallium phosphide directly into the metal surface rather than using a precursor gas such as phosphine during the ablation greatly improved radical yields for the metal phosphides. For the ZnP and ^{67}ZnP radicals, the values for the following magnetic parameters were derived: $g_\perp$, $A_\perp$(P), $A_\perp(^{67}\text{Zn})$, and D. Estimates were made for the following ZnP/^{67}ZnP magnetic parameters: $g_\parallel$, $A_\parallel$(P), and $A_\parallel(^{67}\text{Zn})$. In agreement with theoretical work, the ZnP radical was found to have a $^4\Sigma$ ground state. Several magnetic parameters for the CdP/^{111}CdP/^{113}CdP radicals were also determined: $g_\perp$, $A_\perp$(P), $A_\perp(^{111}\text{Cd})$, and $A_\perp(^{113}\text{Cd})$. Evidence for the formation of the MgP radical was obtained at a field suggestive of a $^4\Sigma$ ground state.

The FACM was used to determine the unpaired electron spin density distribution for the ZnP radical. Two of the unpaired electrons were assumed to be in the phosphorus $3p_x$ and $3p_y$ atomic orbitals. The remaining unpaired electron spin density could then be determined for the phosphorus 3s and $3p_z$ and the zinc 4s and $4p_z$ orbitals. *Ab initio* methods were performed to give estimates of the hyperfine coupling constants for the ZnP radical. The $A_{iso}(^{67}\text{Zn})$ value calculated for all (except MP2) levels of theories was within the experimental uncertainty. In agreement with experimental data, a small $A_{dip}(^{67}\text{Zn})$ value was also predicted by all methods of theory, MRSDCI and SDCI gave the closest estimates. There was poor agreement between theoretical and experimental hyperfine coupling constants for the phosphorus atom. This discrepancy between experimental and theoretical parameters has been seen in previous radicals studied by this group.

The potential energy surfaces were constructed for the seven lowest lying electronic states of the ZnP and MgP radicals using the MCSCF technique. The degeneracy of some states resulted in only five independent states being calculated. Both radicals were found to have $^4\Sigma^-$ ground states. The energy separations, binding energies, bond lengths, dissociation energies, and leading configurations have been reported at r_e. The PESs for the radicals studied exhibit very similar features. The only significant difference is the energy separation of the low-lying electronic states and the significant mixing seen in MgP compared to the ZnP radical. These most likely arise from the energy difference of the valence atomic orbitals of the metal atoms.

ACKNOWLEDGMENTS

We wish to thank Professor T. H. Dunning, Jr. (Pacific Northwest National Laboratory) for providing us with the basis sets and Dr. David Feller and Professor E. R. Davidson for use of their MELDF program. A.J.M. thanks the Australian Research Council for support of this work under the small grants scheme.

[1] *Electrical and Optical Properties of III-V Semiconductors*, edited by N. G. Basov and A. Tybulewicz (Consultants Bureau, New York, 1978) (translated from Russian).
[2] H. C. Freyhardt, *III-V Semiconductors* (Springer-Verlag, Berlin, 1980).
[3] S. J. Pearton, C. R. Abernathy, and F. Ren, *Topics in Growth and Device Processing of III-V Semiconductors* (World Scientific, Singapore, 1996).
[4] S. Sadao, *Properties of Semiconductor Alloys: Group-IV, III-V and II-VI Semiconductors* (John Wiley & Sons, Ltd., Chichestor, 2009).
[5] S. C. O'brien, Y. Liu, Q. Zhang, J. R. Heath, F. K. Tittel, R. F. Curl, and R. E. Smalley, J. Chem. Phys. **84**, 4074 (1986).
[6] S. Li, R. J. Van Zee, and W. Weltner, Jr., J. Phys. Chem. **97**, 11393 (1993).
[7] S. Li, R. J. Van Zee, and W. Weltner, Jr., J. Phys. Chem. **98**, 2275 (1994).
[8] C. S. Xu, E. Debeer, D. W. Arnold, C. C. Arnold, and D. M. Neumark, J. Chem. Phys. **101**, 5406 (1994).
[9] A. P. Alivisatos, J. Phys. Chem. **100**, 13226 (1996).
[10] H. Gómez, T. R. Taylor, Y. Zhao, and D. M. Neumark, J. Chem. Phys. **117**, 8644 (2002).
[11] Z. Cao, B. Suo, and K. Balasubramanian, Chem. Phys. Lett. **432**, 50 (2006).
[12] E. F. Schubert, in *Doping in III-V Semiconductors*, edited by H. Ahmed, M. Pepper, and A. Broers (Cambridge University Press, Cambridge, 2005).
[13] E. Karakyriakos, J. R. Davis, C. J. Wilson, S. A. Yates, A. J. McKinley, L. B. Knight, Jr., R. Babb, and D. J. Tyler, J. Chem. Phys. **110**, 3398

(1999).
[14] A. J. McKinley, E. Karakyriakos, L. B. Knight, Jr., R. Babb, and A. Williams, J. Phys. Chem. A **104**, 3528 (2000).
[15] A. J. McKinley and E. Karakyriakos, J. Phys. Chem. A **104**, 8872 (2000).
[16] E. Karakyriakos and A. J. McKinley, J. Phys. Chem. A **108**, 4619 (2004).
[17] A. I. Boldyrev and J. Simons, J. Phys. Chem. **97**, 6149 (1993).
[18] A. I. Boldyrev and J. Simons, Mol. Phys. **92**, 365 (1997).
[19] M. W. Schmidt and M. S. Gordon, Annu. Rev. Phys. Chem. **49**, 233 (1998).
[20] K. Balasubramanian, J. Chem. Phys. **87**, 3518 (1987).
[21] P. Y. Feng and K. Balasubramanian, Chem. Phys. Lett. **265**, 41 (1997).
[22] P. Y. Feng and K. Balasubramanian, Chem. Phys. Lett. **265**, 547 (1997).
[23] P. Y. Feng and K. Balasubramanian, Chem. Phys. Lett. **283**, 167 (1998).
[24] P. Y. Feng and K. Balasubramanian, Chem. Phys. Lett. **284**, 313 (1998).
[25] P. Y. Feng and K. Balasubramanian, Chem. Phys. Lett. **318**, 417 (2000).
[26] C.-S. Wang and K. Balasubramanian, Chem. Phys. Lett. **402**, 294 (2005).
[27] Z. Cao and K. Balasubramanian, J. Theor. Comput. Chem. **7**, 751 (2008).
[28] B. Manna and K. K. Das, J. Phys. Chem. A **102**, 9876 (1998).
[29] B. Manna, A. Dutta, and K. K. Das, J. Mol. Struct.: THEOCHEM **467**, 135 (1999).
[30] B. Manna, A. Dutta, and K. K. Das, J. Mol. Struct.: THEOCHEM **497**, 123 (2000).
[31] A. Dutta, A. Chattopadhyay, and K. K. Das, J. Phys. Chem. A **104**, 9777 (2000).
[32] B. Manna, A. Dutta, and K. K. Das, J. Phys. Chem. A **104**, 2764 (2000).
[33] A. Dutta, D. Giri, and K. K. Das, J. Phys. Chem. A **105**, 9049 (2001).
[34] A. Chattopadhyay, S. Chattopadhyay, and K. K. Das, J. Phys. Chem. A **106**, 2685 (2002).
[35] A. Chattopadhyay, S. Chattopadhyay, and K. K. Das, J. Mol. Struct.: THEOCHEM **625**, 95 (2003).
[36] A. Chattopadhyay and K. K. Das, J. Phys. Chem. A **107**, 6047 (2003).
[37] A. Chattopadhyay and K. K. Das, J. Phys. Chem. A **108**, 7306 (2004).
[38] L. B. Knight, Jr., J. Steadman, P. K. Miller, and J. A. Cleveland, Jr., J. Chem. Phys. **88**, 2226 (1988).
[39] L. B. Knight, Jr., S. T. Cobranchi, and E. Earl, J. Chem. Phys. **88**, 7348 (1988).
[40] M. W. Schmidt, K. K. Baldridge, J. A. Boatz, S. T. Elbert, M. S. Gordon, J. J. Jensen, S. Koseki, N. Matsunaga, K. A. Nguyen, S. Su, T. L. Windus, M. Dupuis, and J. A. Montgomery, J. Comput. Chem. **14**, 1347 (1993).
[41] T. H. Dunning, Jr., J. Chem. Phys. **90**, 1007 (1989).
[42] R. A. Kendall, T. H. Dunning, Jr., and R. J. Harrison, J. Chem. Phys. **96**, 6796 (1992).
[43] D. E. Woon and T. H. Dunning, Jr., J. Chem. Phys. **98**, 1358 (1993).
[44] D. E. Woon and T. H. Dunning, Jr., J. Chem. Phys. **100**, 2975 (1994).
[45] D. E. Woon and T. H. Dunning, Jr., J. Chem. Phys. **103**, 4572 (1995).
[46] A. J. H. Wachters, J. Chem. Phys. **52**, 1033 (1970).
[47] A. D. McLean and G. S. Chandler, J. Chem. Phys. **72**, 5639 (1980).
[48] MELDF was originally written by L. McMurchie, S. Elbert, S. Langoff, and E. R. Davidson. It has been substantially modified by D. Feller, R. Cave, D. Rawlings, R. Frey, R. Daasch, L. Mitzche, P. Philips, K. Iberle, C. Jackels, and E. R. Davidson.
[49] *Methods of Electronic Structure Theory*, edited by H. F. Schaefer III (Plenum, New York, 1977), Vol. 3.
[50] W. Weltner, Jr., *Magnetic Atoms and Molecules* (Van Nostrand Reinhold, New York, 1989).
[51] W. Weltner, Jr., R. J. Van Zee, and S. Li, J. Chem. Phys. **99**, 6277 (1995).
[52] See supplementary material at http://dx.doi.org/10.1063/1.3491501 for for simulated ZnP spectra superimposed on θ vs B plot; a comparison of calculated and experimental energies; a comparison of ZnP xy_1 from different experimental techniques.
[53] L. B. Knight, Jr. and J. O. Herlong, J. Chem. Phys. **91**, 69 (1989).
[54] W. C. Martin and R. Zalubas, J. Phys. Chem. Ref. Data **1**, 9 (1980).
[55] W. C. Martin, R. Zalubas, and A. Musgrove, J. Phys. Chem. Ref. Data **14**, 751 (1985).
[56] J. Sugar and A. Musgrove, J. Phys. Chem. Ref. Data **24**, 1803 (1995).
[57] A. C. Stowe, J. G. Kaup, L. B. Knight, Jr., J. R. Davis, and A. J. McKinley, J. Chem. Phys. **115**, 4632 (2001).
[58] S. Bililign, J. G. Kaup, and W. H. Breckenridge, J. Phys. Chem. **99**, 7878 (1995).
[59] D. Feller, J. Chem. Phys. **93**, 579 (1990).
[60] L. B. Knight, Jr., S. T. Cobranchi, J. T. Petty, E. Earl, D. Feller, and E. R. Davidson, J. Chem. Phys. **90**, 690 (1989).
[61] J. C. Slater, Phys. Rev. **98**, 1039 (1955).
[62] A. Kalemos, A. Mavridis, and A. Metropoulos, J. Chem. Phys. **116**, 6529 (2002).
[63] H.-J. Werner and W. Meyer, J. Chem. Phys. **74**, 5794 (1981).